International Journal of Plasticity 26 (2010) 925–938

Contents lists available at ScienceDirect

International Journal of Plasticity

journal homepage: www.elsevier.com/locate/ijplas

A dislocation density-based single crystal constitutive equation

M.G. Lee [a], H. Lim [b], B.L. Adams [c], J.P. Hirth [d], R.H. Wagoner [b,*]

[a] Graduate Institute of Ferrous Technology, Pohang University of Science and Technology, San 31 Hyoja-dong, Nam-gu, Pohang, Gyeongbuk 790-784, Republic of Korea
[b] Department of Materials Science and Engineering, The Ohio State University, 2041 College Road, Columbus, OH 43210, USA
[c] Department of Mechanical Engineering, Brigham Young University Provo, UT 84601, USA
[d] 114 E. Ramsey Canyon Road, Hereford, AZ 85615, USA

ARTICLE INFO

Article history:
Received 25 February 2009
Received in final revised form 3 November 2009
Available online 16 November 2009

Keywords:
Single crystal
Dislocation density
Constitutive equation
Orowan hardening

ABSTRACT

Single crystal constitutive equations based on dislocation density (SCCE-D) were developed from Orowan's strengthening equation and simple geometric relationships of the operating slip systems. The flow resistance on a slip plane was computed using the Burger's vector, line direction, and density of the dislocations on all other slip planes, *with no adjustable parameters*. That is, the latent/self-hardening matrix was determined by the crystallography of the slip systems alone. The multiplication of dislocations on each slip system incorporated standard 3-parameter dislocation density evolution equations applied to each slip system independently; this is the only phenomenological aspect of the SCCE-D model. In contrast, the most widely used single crystal constitutive equations for texture analysis (SCCE-T) feature 4 or more adjustable parameters that are usually back-fit from a polycrystal flow curve. In order to compare the accuracy of the two approaches to reproduce single crystal behavior, tensile tests of single crystals oriented for single slip were simulated using crystal plasticity finite element modeling. Best-fit parameters (3 for SCCE-D, 4 for SCCE-T) were determined using either multiple *or* single slip stress–strain curves for copper and iron from the literature. Both approaches reproduced the data used for fitting accurately. Tensile tests of copper and iron single crystals oriented to favor the remaining combinations of slip systems were then simulated using each model (i.e. multiple slip cases for equations fit to single slip, and vice versa). In spite of fewer fit parameters, the SCCE-D predicted the flow stresses with a standard deviation of 14 MPa, less than one half that for the SCCE-T conventional equations: 31 MPa. Polycrystalline texture simulations were conducted to compare predictions of the two models. The predicted polycrystal flow curves differed considerably, but the differences in texture evolution were insensitive to the type of constitutive equations. The SCCE-D method provides an improved representation of single-crystal plastic response with fewer adjustable parameters, better accuracy, and better predictivity than the constitutive equations most widely used for texture analysis (SCCE-T).

1. Introduction

Modern "texture analysis" routinely predicts the plastic anisotropy and texture evolution of polycrystals during large deformation, particularly for FCC crystal structures. Such calculations make use of single-crystal constitutive equations based on slip systems and statistical grain orientation information. The procedure does not consider specific neighboring grain interactions or the presence of grain boundaries, as illustrated in Fig. 1. The linkage among grains in texture analyses is based

* Corresponding author. Tel.: +1 614 292 2079; fax: +1 614 292 6530.
E-mail address: wagoner.2@osu.edu (R.H. Wagoner).

0749-6419/$ - see front matter © 2009 Elsevier Ltd. All rights reserved.
doi:10.1016/j.ijplas.2009.11.004

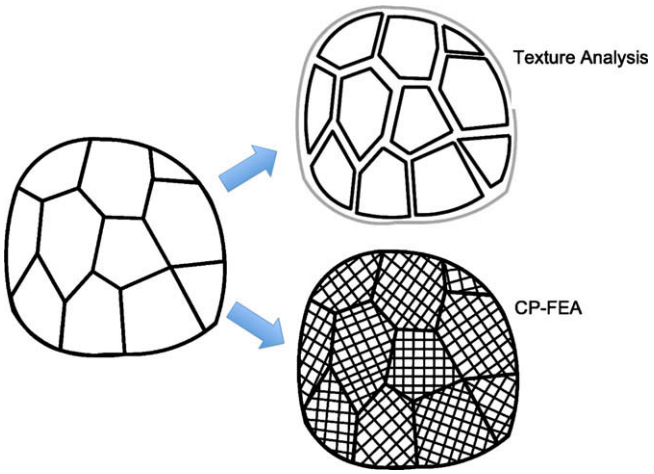

Fig. 1. Schematic view of typical texture analysis and crystal plasticity finite element analysis (CP-FEA). Texture analysis imposes highly-simplified inter-grain rules while CP-FEA imposes compatibility and equilibrium in a finite element sense.

on numerical convenience, assuming that all grains exhibit identical strains (Taylor, 1938), or stresses (Sachs, 1928), or combinations of stress and strain components (Canova et al., 1985). Such models enforce some aspects of inter-grain equilibrium or compatibility, but not both (Parks and Ahzi, 1990). An alternative formulation treats a single grain as an inclusion within a homogenized medium (Kröner, 1961; Molinari et al., 1987).

Crystal-plasticity finite element analysis (CP-FEA) (Peirce et al., 1982; Asaro, 1983; Dawson, 2000) enforces inter-grain equilibrium and compatibility in a finite element sense (with many elements in a single grain), thus treating the interactions among neighboring grains more realistically (Raabe et al., 2002), Fig. 1, but with large penalties in computation time. Recent applications of CP-FEA have been extended to the deformation of single, bi- and polycrystals (Zaefferer et al., 2003; Ma et al., 2006; Zaafarani et al., 2006; Raabe et al., 2007), incorporating size dependence through strain gradient terms (Abu Al-Rub and Voyiadijus, 2005) and nanoindentation simulations (Wang et al., 2004; Liu et al., 2005, 2008). These methods are too CPU-intensive for use with large grain assemblies (i.e. typical polycrystals) or for treating applied deformation boundary-value problems. Modifications to improve the efficiency of the calculations limit the accuracy by, for example, applying iso-strain conditions within a grain (Kalidindi et al., 1992; Dawson et al., 2003) or having each finite element represent a single grain (Nakamachi et al., 2001).

Polycrystal simulations, whether of the texture-type or CP-FEA type, use single crystal plasticity constitutive models based on slip system activity. Typical formulations are either elastic-plastic rate-independent (Mandel, 1965; Hill, 1966; Rice, 1971; Hill and Rice, 1972; Asaro and Rice, 1977; Asaro, 1983; Anand and Kothari, 1996; Marin and Dawson, 1998) or viscoplastic (Peirce et al., 1982; Asaro and Needleman, 1985). This viscoplastic approach has recently been referred to in the literature as "PAN" (e.g. Thakare et al., 2009; Patil et al., 2008; Alcalá et al., 2008), named for "Peirce, Asaro, Needleman" (Peirce et al., 1982; Asaro and Needleman, 1985). The PAN approach uses an arbitrary small strain rate sensitivity index to avoid numerical non-uniqueness. The most commonly used PAN formulation relies on a power-law equation relating shear stress to shear strain rate on each slip system (Asaro and Needleman, 1985) with the slip system resistance evolving with total slip on each slip system according to latent and self-hardening (Mandel, 1965; Hill, 1966).

The adjustable parameters in the single-crystal constitutive equations used for texture analysis are almost universally determined by back-fitting them to mechanical test results (i.e. uniaxial tension or compression) of macroscopic polycrystals that are simulated using the same technique for which the constitutive equations are destined. Such a procedure guarantees that the macroscopic tests used to fit the parameters are reproduced accurately by the simulations, *but not that the single-crystal constitutive equations represent true single-crystal behavior.* Simulations of problems based on such an approach have proven useful for a range of strain, strain rates, and temperatures (Mathur and Dawson, 1989; Bronkhorst et al., 1992; Beaudoin et al., 1994; Kumar and Dawson, 1998; Nemat-Nasser et al., 1998). However, there is evidence that single-crystal plasticity models fitted in this way do not always represent single-crystal behavior properly (Becker and Panchanadeeswaran, 1995; Kumar and Yang, 1999; Arsenlis and Parks, 2002). If the presence and characterization of grain boundaries (and grain shape, size, misorientation, etc.) influences the relationship between single-crystal and polycrystal deformation characteristics, the standard back-fitting procedure evidently would not yield a correct description of single-crystal behavior. Instead, the single-crystal constitutive equations embed undetermined aspects of the inter-grain interactions and thus, may not represent single crystal behavior but rather some amalgam of single and polycrystal aspects. One of the purposes of the current work is to determine whether the predominant formulation of **s**ingle-**c**rystal **c**onstitutive **e**quations used for a wide range of successful **t**exture calculations ("SCCE-T") captures single crystal behavior properly, particularly single slip vs. multiple slip. The answer to that question bears on the question of whether inter-grain interactions are incorporated in an unknown way into the SCCE-T's fit to macroscopic observations.

Note: "SCCE-T" refers in this paper to a set of choices within the broader PAN framework. It is SCCE-T that is used with wide success in texture calculations appearing in the literature. SCCE-T is a subset of PAN, the latter of which has greater flexibility with a commensurate number of additional adjustable parameters. As a particular example, the majority of successful texture calculations use a fixed value, 1.4, describing the ratio of latent hardening to self-hardening that agrees with experience at the macro/texture level. SCCE-T, in addition to having the validation of wide testing over more than 20 years, has only one additional parameter compared with the constitutive model proposed here. Thus, comparisons between the two are meaningful. Summaries of the constitutive forms considered in this paper are presented later.

Alternate developments to represent single-crystal behavior based on dislocation densities have appeared. Models of this type typically exhibit considerable complexity and large numbers of undetermined parameters. Models based on statistical aspects of dislocation densities represented as internal state variables (Ortiz et al., 1999; Arsenlis and Parks, 2002) captured the orientation-dependent flow behavior of FCC single crystals. Developments for FCC and BCC single crystals make use of Orowan's equation (Orowan, 1940) and have incorporated many physical complexities, including dislocation velocities, activation energies, and dislocation walls (Roters et al., 2000). In order to reproduce the compression of aluminum single crystals at elevated temperature, 8 fit parameters and 2 activation energies were required to predict stress strain curves for a range of strain rates and temperatures in one study (Ma et al., 2004).

In the current work, a **d**islocation-based **s**ingle **c**rystal **c**onstitutive **e**quation ("SCCE-D") is newly formulated with 3 undetermined parameters corresponding to a standard equation representing the evolution of dislocation density. The form is similar to standard corresponding texture-type equations, except that the dislocation density for each slip system and its evolution is used explicitly rather than implicitly via slip system strength and its evolution with total slip (Ortiz and Popov, 1982; Brown et al., 1989; Kalidindi et al., 1992; Kuchnicki et al., 2006; Wang et al., 2007). Use of physical dislocation densities allows application of Orowan's strengthening model (Orowan, 1948) to determine the cross-hardening effects without undetermined parameters (see also Bassani and Wu, 1991; Liu et al., 2008). Such cross-hardening effects depend on the geometry of the crystal lattice type, not on undetermined parameters.

Tests of SCCE-D are made for single-crystal and polycrystal deformation and the results are compared with corresponding ones using standard SCCE-T. We emphasize that we have selected the SCCE-T for comparison with the new model because it dominates successful texture calculations presented in the literature. As such, it represents an informal "consensus" of what has been found to work. None of the other variants within the PAN formalism approach the breadth of experience or acceptance in the community. The question to be answered is whether the SCCE-T formulation that finds broad success for polycrystal simulations represents single-crystal behavior properly, and if not, whether a less-adjustable/more predictive formulation can improve on the single-crystal representation. A secondary question is how such an alternative formulation would affect macroscopic texture calculations.

2. Crystal plasticity based on single crystal constitutive equations

The kinematics for either SCCE-T or SCCE-D are based on well-established developments (Lee, 1969; Rice, 1971; Hill and Rice, 1972; Asaro and Rice, 1977; Peirce et al., 1982). The total deformation gradient is decomposed into elastic and plastic parts (Lee, 1969):

$$\mathbf{F} = \mathbf{F}^{\mathrm{e}}\mathbf{F}^{\mathrm{p}} \tag{1}$$

where $\mathbf{F}^{\mathrm{e}}$ corresponds to elastic distortion of lattice, and $\mathbf{F}^{\mathrm{p}}$ defines the slip by the dislocation motion in the unrotated configuration (Mandel, 1965).

The plastic velocity gradient in the unrotated (or intermediate) configuration is:

$$\bar{\mathbf{L}}^{\mathbf{p}} = \dot{\mathbf{F}}^{\mathbf{p}}\mathbf{F}^{\mathbf{p}-\mathbf{1}} \tag{2}$$

The evolution of the plastic deformation can be expressed as the sum of all crystallographic slip rates, $\dot{\gamma}^{\alpha}$ (Rice, 1971),

$$\bar{\mathbf{L}}^{\mathbf{p}} = \sum_{\alpha=\mathbf{1}}^{\mathbf{n}} \dot{\gamma}^{\alpha}\mathbf{s}_{\mathbf{0}}^{\alpha} \otimes \mathbf{n}_{\mathbf{0}}^{\alpha} \tag{3}$$

where $\mathbf{s}_0^{\alpha}$ and $\mathbf{n}_0^{\alpha}$ are the vectors representing slip direction and slip plane normal of the slip system α, respectively and n is total number of slip systems.

2.1. Common elements of SCCE-T and SCCE-D

For a rate-dependent crystal plasticity model, the plastic shear rate of each slip system α is typically expressed as a power-law function of the resolved shear stress τ^{α} as (Hutchinson, 1976; Peirce et al., 1982):

$$\dot{\gamma}^{\alpha} = \dot{\gamma}_0 \left(\frac{\tau^{\alpha}}{g^{\alpha}}\right)^{\frac{1}{m}} \mathrm{sign}(\tau^{\alpha}) \tag{4}$$

where $\dot{\gamma}_0$ is reference shear rate, g^{α} is the slip resistance (or flow stress) of the slip system α and m is the rate sensitivity exponent. The initial flow stress is generally assumed to be the same, i.e. g_0, for all slip systems. Reference shearing rate

and rate sensitivity, 0.001 s^{-1} and 0.012, respectively, are adopted from the literature (Bronkhorst et al., 1992; Kalidindi et al., 1992).

To complete the constitutive equations, the second Piola-Kirchhoff stress is defined as follows, and is related elastically to the strain:

$$\mathbf{S} = \mathbf{C}^{e} : \mathbf{E} = \det(\mathbf{F}^{e})\mathbf{F}^{e-1}\sigma\mathbf{F}^{e-T} \tag{5}$$

where $\mathbf{E} = \frac{1}{2}(\mathbf{F}^{eT}\mathbf{F}^{e} - \mathbf{I})$ is the Lagrangian strain tensor, σ is the Cauchy stress, and $\mathbf{C}^{e}$ is the fourth order elastic constant matrix.

The resolved shear stress of slip system α in Eq. (4) is approximately,

$$\tau^{\alpha} = \mathbf{S} : \mathbf{P}_0^{\alpha} \equiv \mathbf{S} : (\mathbf{s}_0^{\alpha} \otimes \mathbf{n}_0^{\alpha}) \quad \text{or} \quad \tau^{\alpha} = \mathbf{S_{ij}}\mathbf{P}_{\mathbf{0ij}}^{\alpha} \equiv \mathbf{S_{ij}} : (\mathbf{s}_{\mathbf{0i}}^{\alpha}\mathbf{n}_{\mathbf{0j}}^{\alpha}) \tag{6}$$

The slip resistance (equivalent to a critical resolved shear stress (CRSS) for a rate-independent elastic-plastic law) of slip system α, g^{α} evolves as the slip (or gliding) of dislocations on the slip system occurs. The governing rule of the evolution of slip resistance (hardening) is a critical aspect of the constitutive framework and causes the SCCE-T and SCCE-D approaches to diverge, as described in the following sections.

2.2. Single-Crystal Constitutive Equations developed for Texture models (SCCE-T)

Texture analyses predominantly utilize phenomenological models for the evolution of flow stress on a slip system α as related to the slip increment on all slip systems β as follows (Asaro, 1983):

$$\dot{g}^{\alpha} = \sum_{\beta} \mathrm{h}_{\alpha\beta}\dot{\gamma}^{\alpha} \tag{7}$$

where $\mathrm{h}_{\alpha\beta}$ are hardening coefficients. Most texture analyses have adopted the following form for the hardening coefficient matrix (Hutchinson, 1976; Asaro, 1979; Peirce et al., 1982):

$$\mathbf{h}_{\alpha\beta} = \mathbf{h}_{\beta}(\mathbf{q_{lat}} + (\mathbf{q_{self}} - \mathbf{q_{lat}})\delta_{\alpha\beta}) \tag{8}$$

where $\delta_{\alpha\beta}$ is the Kronecker delta and $\mathbf{q_{self}}$ and $\mathbf{q_{lat}}$ determine the self and latent hardening, respectively. The hardening matrix contains two distinct values: diagonal terms ($\mathbf{q_{self}}$) for the self-hardening and off-diagonal terms ($\mathbf{q_{lat}}$) for the latent hardening. Experimental observations (Kocks, 1970) suggested that the range $1 \leqslant \mathbf{q_{lat}}/\mathbf{q_{self}} \leqslant 1.4$ applies for FCC single crystals, and $\mathbf{q_{lat}}/\mathbf{q_{self}} = 1.4$ is typically used in texture analyses of FCC polycrystals e.g. (Peirce et al., 1982; Asaro and Needleman, 1985; Mathur and Dawson, 1989; Kalidindi et al., 1992).

The form of $\mathbf{h}_{\beta}$ in Eq. (8) has been proposed to properly represent the stress–strain behavior of polycrystals. Here, the widely used form proposed by Brown et al. (1989)) is adopted:

$$\mathbf{h}_{\beta} = \mathbf{h_0}\left(\mathbf{1} - \frac{g^{\beta}}{g_s}\right)^{\mathrm{a}} \tag{9}$$

where $\mathbf{h_0}$ is the initial hardening rate, g_s is the saturated flow stress and a is the hardening exponent. The initial hardness g_0 is typically fitted to reproduce the macroscopic yield stress. Eqs. (7)–(9) have been shown to predict the stress–strain response and evolution of texture for simple deformation of FCC polycrystals (Mathur and Dawson, 1989; Kalidindi et al., 1992). When the parameters are back-fitted to stress–strain responses of polycrystals, there are 4 arbitrary parameters to be fit from macroscopic polycrystal stress–strain curves to complete Eqs. (7)–(9): $\mathbf{h_0}$, g_s, g_0 and a in Eqs. (4), (8), and (9). These undetermined parameters, $\mathbf{h_0}$, g_s, g_0, and a are typically set from the stress–strain curve for a polycrystal tensile test.

2.3. Single-Crystal Constitutive Equations based on the Dislocation density model (SCCE-D)

In the SCCE-D derived here, the hardening is expressed in terms of the interaction of mobile dislocations with corresponding forest dislocations that act as point obstacles, Fig. 2. These interactions are evaluated using Orowan's strengthening model assuming that forest dislocations are hard pins with respect to intersecting mobile dislocation. That is, the intersection points become immobile and the mobile dislocation must bypass by looping around the obstacle rather than cutting through it. In fact, dislocation intersections are known to be hard pins in most metals at low homologous temperatures (Hirth and Lothe, 1969).

In Orowan's model (Orowan, 1948), if the applied stress is large enough, dislocations loop around an obstacle and will overcome and bypass it, leaving dislocation loops behind. The critical stress (g^{α}) necessary to bow out a dislocation on a slip system α to a radius r is calculated by considering the equilibrium with the line tension of the dislocation, T:

$$g^{\alpha} \cdot b = \frac{T}{r} \tag{10}$$

where b is the Burger's vector. The dislocation is considered to have a line tension equal to its self-energy per unit length and is approximated (Weertman and Weertman, 1992) as follows:

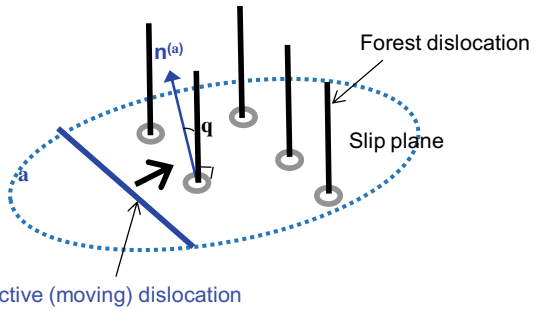

Fig. 2. Interaction between a moving dislocation on an active slip system and corresponding forest dislocation array.

$$T \approx \frac{1}{2}\mu b^2 \tag{11}$$

where μ is shear modulus. Combining Eqs. (10) and (11), we express the critical bypass stress as

$$g^{\alpha} = \frac{\mu b}{2r} = \frac{\mu b}{l} \tag{12}$$

where the critical radius of curvature is set equal to half of the inter-pin spacing. Eq. (12) is the well-known relationship for Orowan's bypass mechanism. If the applied stress exceeds the bypass stress, dislocations bypass the obstacle, allowing long-range plastic straining, and loops are formed around each obstacle. Now we assume that the obstacles are forest dislocations, that is dislocations lying on other slip systems that pierce the slip plane of the α slip system. Since the obstacle spacing distance l, in Eq. (12) depends on the density of forest dislocations, Eq. (12) can be rewritten as:

$$g^{\alpha} = \mu b\sqrt{\rho_f} \tag{13}$$

where ρ_f is the density of dislocations that penetrate the slip plane of slip system α. For the flow stress derived in Eq. (13) assumes that all of the forest dislocation lines are assumed to be parallel to the α slip plane normal. For an arbitrary angle, θ, between the two directions, as shown in Fig. 2, the effective forest dislocation density $\bar{\rho}_f$ is as follows:

$$\bar{\rho}_f = \rho_f \cos\theta = \rho_f \cdot (\mathbf{n}^{\alpha} \cdot \boldsymbol{\xi}_{\mathbf{f}}) \tag{14}$$

where $\mathbf{n}^{\alpha}$ and $\boldsymbol{\xi}_{\mathbf{f}}$ are the slip plane normal of the moving dislocation being considered and the line direction of the corresponding forest dislocation, respectively. The effective forest dislocation density, $\bar{\rho}_f$ is maximized when $\theta = 0^{\circ}$ and vanishes if $\theta = 90^{\circ}$, i.e. if the mobile and forest dislocations are coplanar. Therefore, the flow stress can be represented as:

$$g^{\alpha} = \mu b\sqrt{\rho_{\mathbf{f}} \cdot (\mathbf{n}^{\alpha} \cdot \boldsymbol{\xi}_{\mathbf{f}})} \tag{15}$$

Eq. (15) includes the assumption that all forest dislocations are parallel to each other. To generalize to an array of forest dislocations, the interactions are summed over each type of dislocations/slip system (Franciosi and Zaoui, 1982). If there are n different slip systems, the Eq. (15) becomes:

$$g^{\alpha} = \mu b\sqrt{\sum_{\beta=1}^{n} \mathbf{h}_{\alpha\beta}\rho_{\beta}} \tag{16}$$

where $\mathbf{h}_{\alpha\beta} = \mathbf{n}^{\alpha} \cdot \boldsymbol{\xi}^{\beta}$ is given by the geometries of edge dislocations for each slip system, with no undetermined parameters.

To complete the SCCE-D development, a widely used dislocation density evolution equation based on slip systems is adopted (Kocks, 1976).

$$\dot{\rho}^{\alpha} = \frac{1}{b}\left(\frac{\sqrt{\sum_{\beta}^{n}\rho^{\beta}}}{k_a} - k_b\rho^{\alpha}\right) \cdot |\dot{\gamma}^{\alpha}| \tag{17}$$

where k_a and k_b are material parameters for the generation and annihilation terms of dislocations, respectively. The final SCCE-D defined by Eq. (16) and (17) has three parameters to be determined, each of them related to dislocation density and its evolution: k_a, k_b and ρ_0.

3. Results and discussion

In order to compare the accuracy and usefulness of SCCE-T and SCCE-D as described above, the adjustable parameters were fit to reproduce the measured stress–strain response of single crystals oriented for either multiple or single slip. The

Table 1
Best-fit parameters and range of parameters for fitting SCCCE-T and SCCE-D.

Best fit parameters		SCCE-T				Std. error of fit (MPa)	SCCE-D			Std. error of fit (MPa)
	Fit direction	g_0 (MPa)	g_s (MPa)	$\mathbf{h}_0$ (MPa)	a		ρ_0 (mm^{-1})	k_a	k_b	
Cu	[0 0 1]	1	89	255	1	0.67	10^3	22	33.5[a]	0.64
	[−1 2 3]	1	58	37	−0.75	2.10	10	51	3[a]	1.65
Fe	[0 0 1]	18	81	141	0.25	0.41	2.5×10^5	59	4[a]	0.77
	[−3 4 8]	18	58	17	−1.25	0.29	2.5×10^5	156	0.5[a]	1.89
Fit procedure parameters										
Data range		*	0–300	0–300	−3 to 3		*	1–200	0–50[a]	
Increment 1		–	10	10	1		–	10	10[a]	
Increment 2		–	1	1	0.25		–	1	0.5[a]	

[a] Burgers vector (=0.257 nm).
* Obtained by simple trial and error.

Table 2
Anisotropic elasticity constants for single crystal copper (Simmons and Wang, 1971) and iron (Hirth and Lothe, 1969) (unit: GPa).

	C_{11}	C_{12}	C_{44}	Shear modulus (μ)
Cu	170	124	75	48
Fe	242	150	112	80

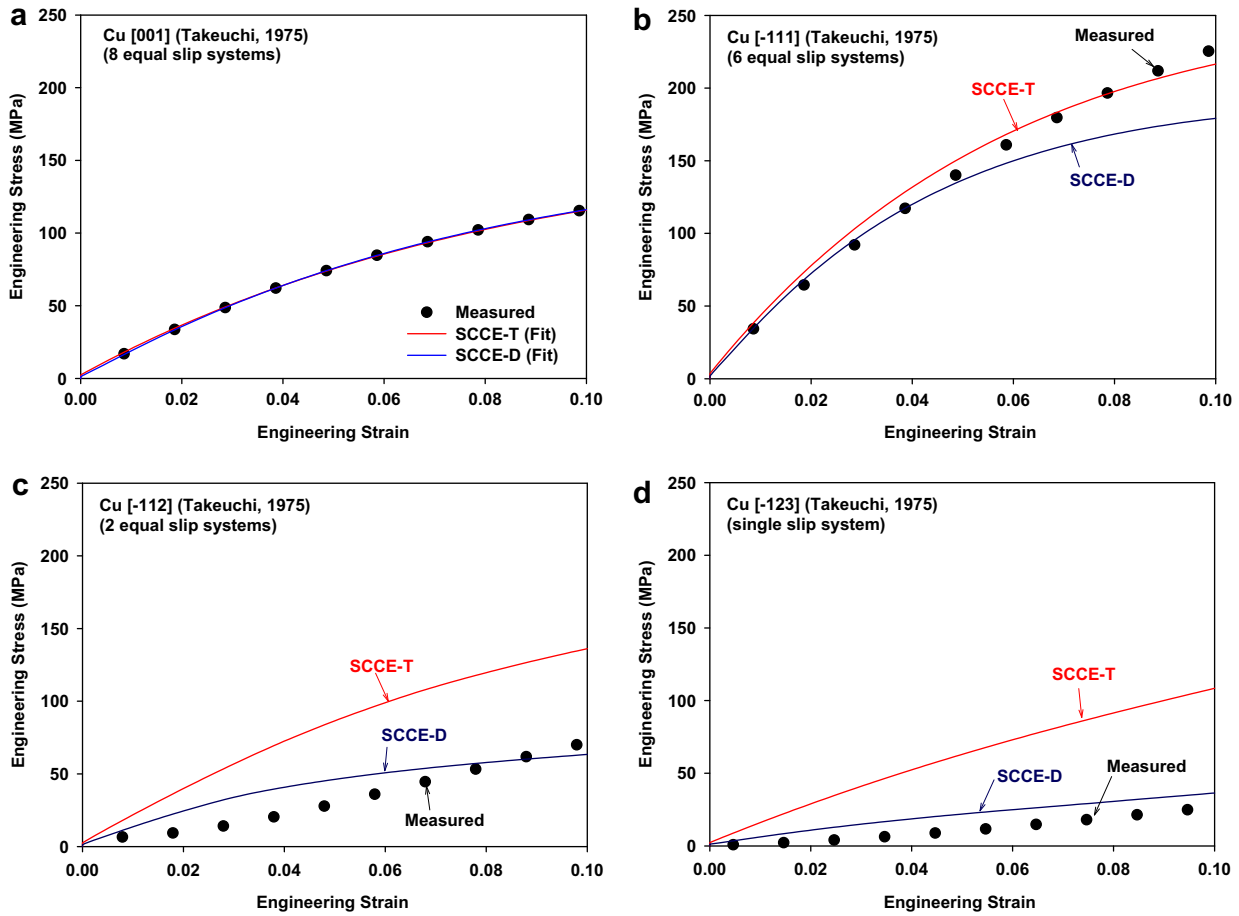

Fig. 3. Comparison of stress–strain curves from SCCE-T and SCCE-D constitutive models and measurements from the literature (Takeuchi, 1975) for copper single crystals with tensile axes in the following orientations: (a) [0 0 1] (b) [−1 1 1] (c) [−1 1 2] (d) [−1 2 3]. The parameters for the SCCE-T and SCCE-D constitutive models have been fitted to the [0 0 1] tensile test results, as shown in part (a).

resulting material models were then used with finite element modeling to predict the stress–strain response for tensile tests oriented for the activation of other combinations of slip systems. The predicted responses were then compared with corresponding experimental results from the literature.

3.1. CP-FEM implementation

The two single-crystal constitutive equations described in the previous section were implemented into the commercial finite element program ABAQUS/Standard via the user material subroutine, UMAT (Hibbit, 2005). A single eight-noded con-

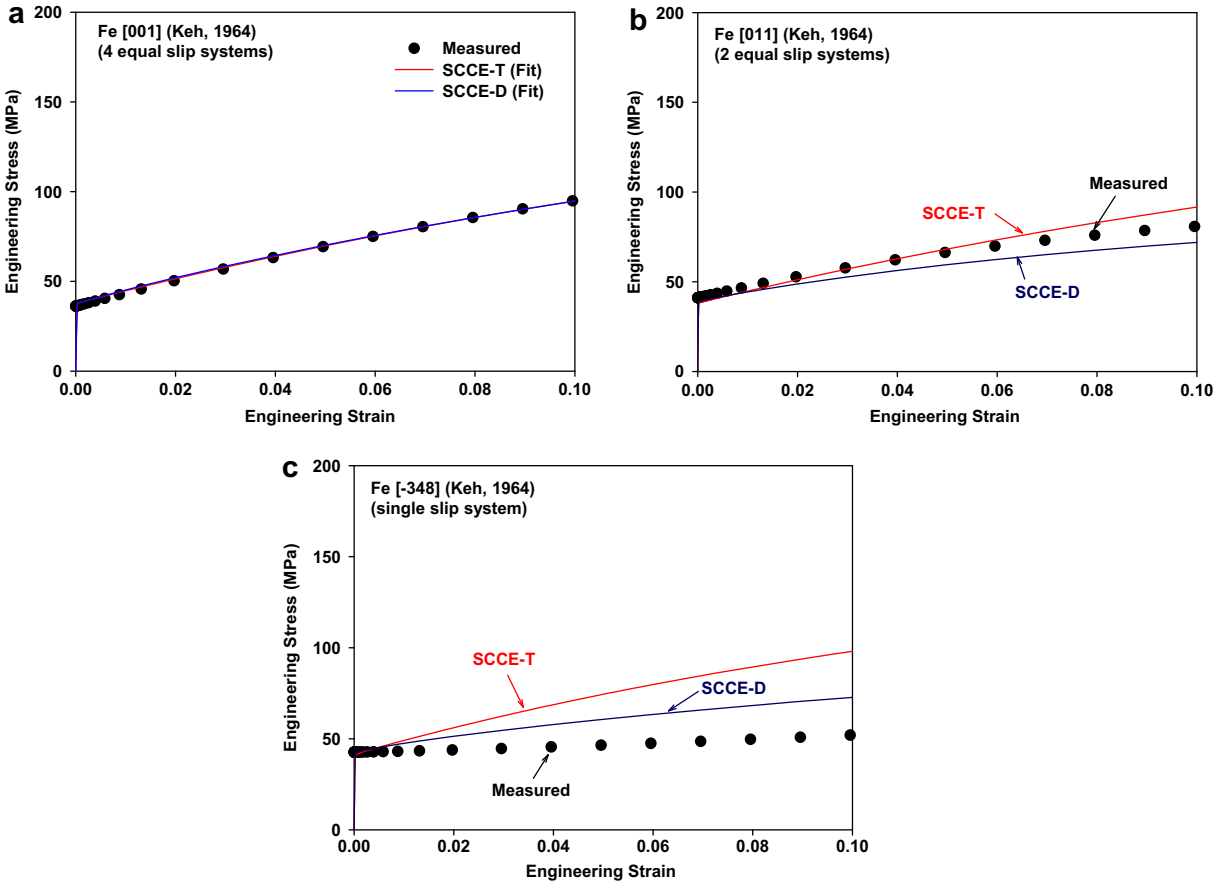

Fig. 4. Comparison of stress–strain curves from SCCE-T and SCCE-D constitutive models and measurements from the literature (Keh, 1965) for iron single crystals with tensile axes in the following orientations: (a) [0 0 1] (b) [0 1 1] (c) [−3 4 8]. The parameters for the SCCE-T and SCCE-D constitutive models have been fitted to the [0 0 1] tensile test results, as shown in part (a).

Table 3
Standard deviations and error percentage[a] between predicted and measured stress–strain curves.

	Fit direction	Tensile axis direction	SCCE-T	SCCE-D
Cu	[0 0 1]	[1 1 1]	8 (6%)	23 (16%)
		[−1 1 2]	54 (150%)	13 (35%)
		[−1 2 3]	58 (451%)	10 (79%)
Fe	[0 0 1]	[0 1 1]	5 (8%)	7 (11%)
		[−3 4 8]	31 (66%)	15 (31%)
Avg. (multiple slip fit)			**31 (136%)**	**14 (34%)**
Cu	[−1 2 3]	[0 0 1]	62 (82%)	38 (50%)
		[1 1 1]	113 (78%)	79 (55%)
		[−1 1 2]	19 (54%)	7 (20%)
Fe	[−3 4 8]	[0 0 1]	30 (42%)	23 (32%)
		[0 1 1]	24 (36%)	20 (30%)
Avg. (single slip fit)			**50 (58%)**	**33 (37%)**

[a] Error percentage (%) = standard deviation/averaged flow stress × 100.

tinuum element (C3D8) was utilized to simulate the tensile tests of single crystals. The tensile direction was aligned with one of the element axes and the two faces of the cube element were initially perpendicular to the loading axis. During the deformation, the two faces remain parallel to each other and perpendicular to the loading axis, simulating the deformation mode imposed by a stiff tensile machine. Crystallographic slip was considered on the 12 equivalent {1 1 1}⟨1 1 0⟩ slip systems for FCC copper and 12 {1 1 0}⟨1 1 1⟩ and 12 {1 1 2}⟨1 1 1⟩ slip systems for BCC iron.

The tensile stress–strain responses for oriented single crystals have been measured. For FCC copper single crystals, 4 tensile axis orientations are available (Takeuchi, 1975; Arsenlis and Parks, 2002): ⟨1 2 3⟩, ⟨1 1 2⟩, ⟨1 0 0⟩, and ⟨1 1 1⟩. The ⟨1 2 3⟩ tensile axis is oriented for single slip while ⟨1 1 2⟩, ⟨1 1 1⟩ and ⟨1 0 0⟩ tensile axes are oriented for multiple slip, with 2, 6 and 8 equally favored slip systems respectively. For BCC iron single crystals, 3 tensile axis orientations are available (Keh, 1965): ⟨3 4 8⟩, ⟨1 1 0⟩, and ⟨1 0 0⟩. The ⟨3 4 8⟩ tensile axis is oriented for single slip while the ⟨1 1 0⟩ and ⟨1 0 0⟩ tensile axes are orientated for multiple slip, with 2 and 4 equally favored slip systems respectively.

3.2. Prediction of single crystal stress–strain response

SCCE-T and SCCE-D models were fit by comparing FE simulations of single-crystal tensile tests oriented along directions with most equivalent slip systems, [0 0 1], with corresponding experimental stress–strain curves from the literature. The best-fit parameters, Table 1, were determined using the procedure described below. The stress–strain responses for other orientations of tensile axis were then predicted using the resulting constitutive equations. For SCCE-T, h_0 affects the initial hardening rate, g_s determines the final saturated value of stress, g_0 determines initial yield and a affects the shape of the stress–strain curve (Kalidindi et al., 1992). For SCCE-D, ρ_0 corresponds to g_0 for SCCE-T, which determines the yield stress while k_a and k_b affect the shape of the flow curve.

In order to determine the set of parameters with minimum standard error of fit, g_0 for SCCE-T and ρ_0 for SCCE-D were first obtained from the observed yield stress by simple trial and error. Then, a 3D "box" containing an assumed range of all pos-

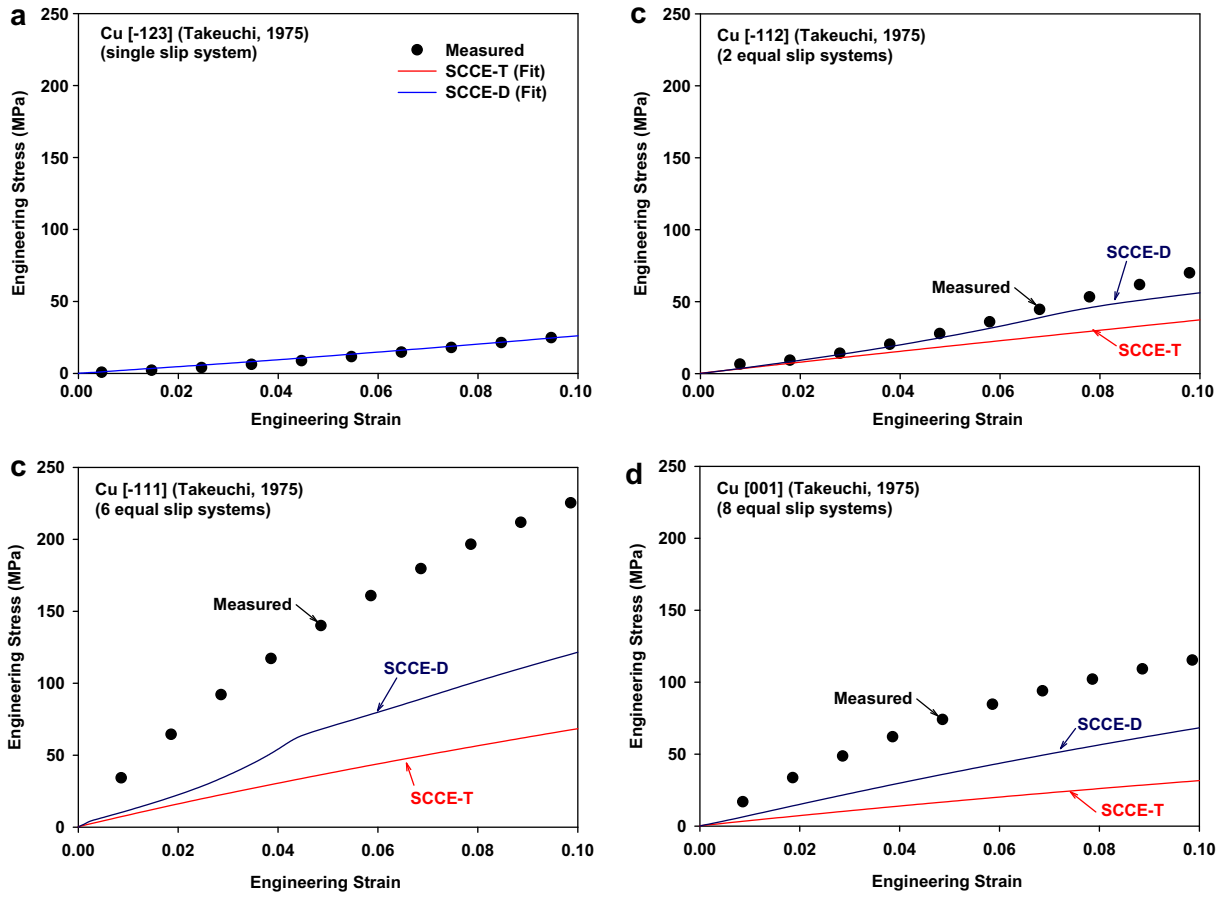

Fig. 5. Comparison of stress–strain curves from SCCE-T and SCCE-D constitutive models and measurements from the literature (Takeuchi, 1975) for copper single crystals with tensile axes in the following orientations: (a) [−1 2 3] (b) [−1 1 2] (c) [−1 1 1] (d) [0 0 1]. The parameters for the SCCE-T and SCCE-D constitutive models have been fitted to the [−1 2 3] tensile test results, as shown in part (a).

sible combinations of parameters was constructed, along with equally-spaced interior points. Using SCCE-T as an example, 6727 equally-spaced interior points (i.e. $31 \times 31 \times 7$) representing 6727 choices of constitutive parameters was considered with ranges and increments as defined in Table 1 (Increment 1). The following steps were then followed:

1. For each of the 6727 choices, a finite element analysis was performed and a standard deviation of stress from the simulation and experiments was determined up to a strain of 0.1. The set of parameters representing the minimum standard deviation was identified for further refinement.
2. The behavior of the standard deviation moving along any parametric axis was examined. For all the cases considered here, the standard deviation increased monotonically in all such directions moving away from the minimum standard deviation set identified in Step 1.

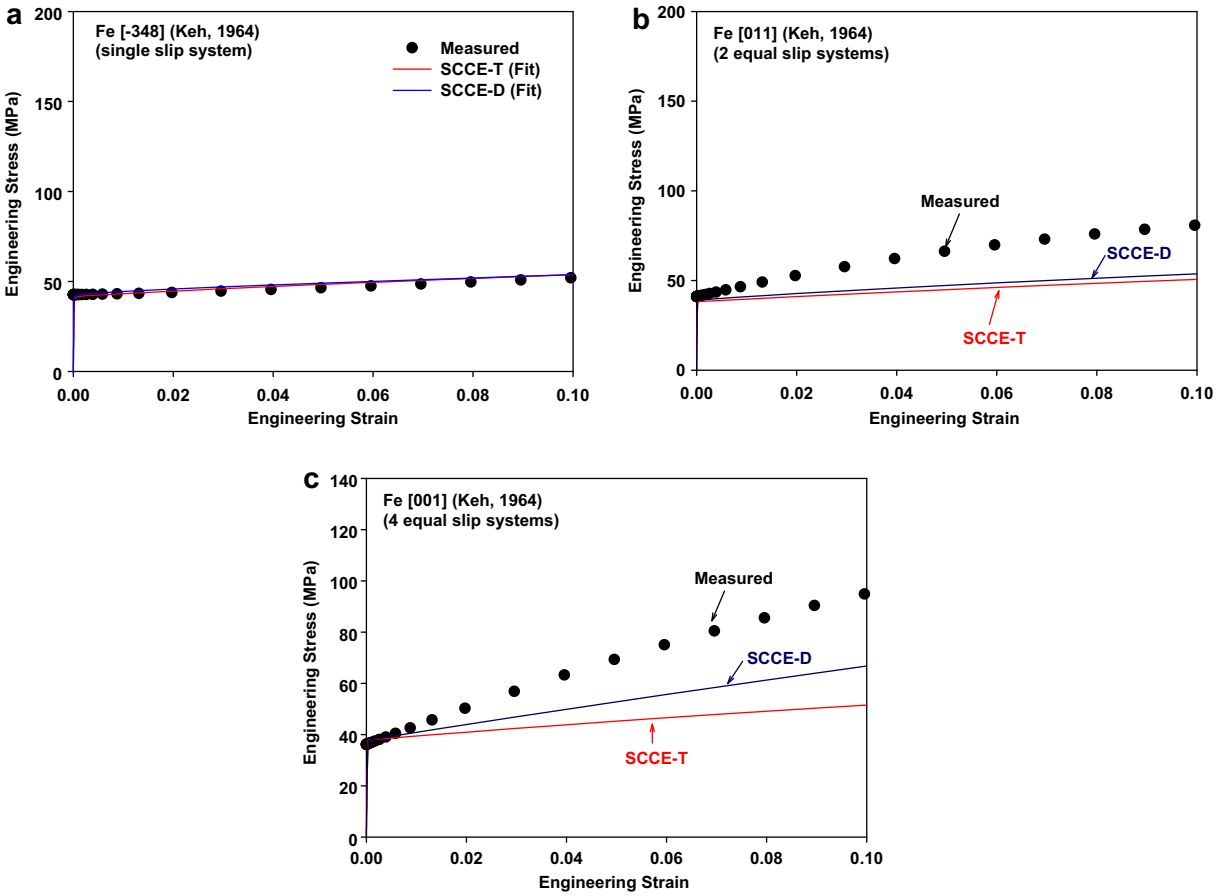

Fig. 6. Comparison of stress–strain curves from SCCE-T and SCCE-D constitutive models and measurements from the literature (Keh, 1965) for iron single crystals with tensile axes in the following orientations: (a) [−3 4 8] (b) [0 1 1] (c) [0 0 1]. The parameters for the SCCE-T and SCCE-D constitutive models have been fitted to the [−3 4 8] tensile test results, as shown in part (a).

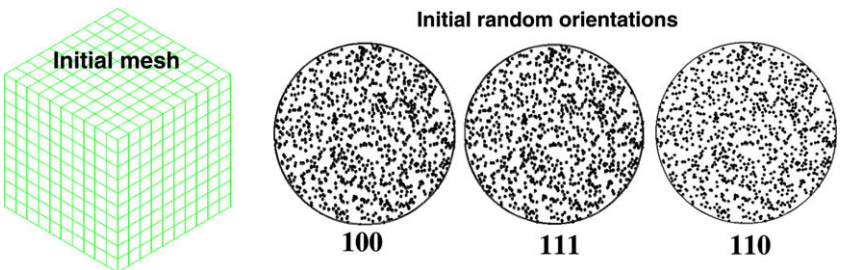

Fig. 7. Initial mesh and pole figures for the initial random orientations used for the finite element simulations.

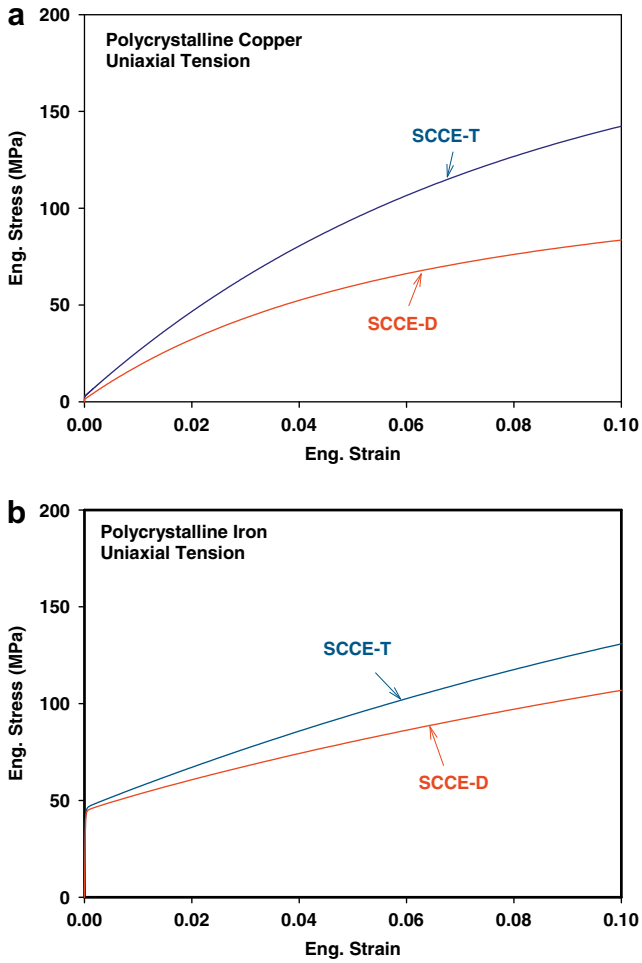

Fig. 8. Simulated macroscopic engineering stress–strain curves for uniaxial tension for (a) polycrystal copper, and (b) polycrystal iron.

3. Starting from the set of parameters identified in Step 1, a smaller set of increments (Increment 2 in Table 1) was used to define 3969 ($21 \times 21 \times 9$) new sets of parameters throughout a range that includes the original cells adjacent to the location of the minimum standard deviation. Step 1 was again carried out using these choices, and the minimum standard deviation was thus refined. Again, the standard deviation was verified to increase monotonically from this set of values moving away from it along any parametric axis.

In this way, a unique set of best-fit constitutive parameters was determined and confidence in its uniqueness established.

Anisotropic elasticity constants and shear modulus for copper and iron single crystals are used in all finite element simulations are shown in Table 2.

Predicted and measured stress–strain curves are compared in Figs. 3 and 4 for copper and iron single crystals, respectively. Figs. 3(a) and 4(a) show the accuracy of SCCE-T and SCCE-D fitted curves as compared to the [0 0 1] experimental data used to fit them. The two approaches fitted the multiple slip [0 0 1] tensile data with approximately the same accuracy (Table 1). Figs. 3(b–d) and 4(b and c) compare the predictions of SCCE-T and SCCE-D models (based on [0 0 1] tensile data) with experimental results for other tensile test directions. The fitting parameters for SCCE-T do not adequately represent the stress–strain response of single crystals, especially for single slip. The likely source of error for SCCE-T is the self/latent hardening ratio, $\mathbf{q_{lat}}/\mathbf{q_{self}} = 1.4$, which corresponds to significant self-hardening. In contrast, the measured hardening rate of the stress–strain curve oriented for single slip is very low, implying negligible self-hardening.[1]

The SCCE-D model agrees better with measurements in spite of having less number of arbitrary parameters. The standard deviations between the measured and predicted results are listed in Table 3. The average standard deviation of measurements to the SCCE-D prediction is 14 MPa while that for the SCCE-T prediction is 31 MPa.

[1] There is some hardening in single slip orientations even without self-hardening because of the rotation of the crystallographic direction relative to the tensile axis toward a less favorable slip orientations (Anand and Kothari, 1996).

To check whether the above conclusions are unique to fitting to multiple slip tensile experiments, we refitted the equations to single slip data, with the results shown in Table 3 and Figs. 5 and 6. The average standard deviation for the SCCE-T model is 50 MPa while that for the SCCE-D model is 33 MPa. The difference in the fit parameters and the standard deviations show that the new approach does not predict perfectly the differences between single slip and multiple slip, but SCCE-D is significantly better, with fewer adjustable parameters, than the standard SCCE-T.

3.3. Comparison of stress–strain response and texture evolution in polycrystalline simulations

Uniaxial compression and tension tests of polycrystalline copper and iron were simulated using SCCE-T and SCCE-D models to examine their role on the predicted stress–strain response and texture evolution of polycrystals. Material properties shown in Table 1 for the [0 0 1] fit were used, along with an FE mesh with a total of 1000 ($10 \times 10 \times 10$) 3-dimensional solid elements, each representing a single grain. An isotropic texture was generated by assigning a random orientation to every element in the form of Bunge's Euler angles. The initial mesh and random crystal orientation as described by equal-area pole figures are shown in Fig. 7.

Figs. 8 and 9 show the simulated stress–strain curves for the SCCE-T model and the SCCE-D model for copper and iron polycrystals. The SCCE-T prediction for both copper and iron polycrystals shows higher flow stresses than SCCE-D predictions

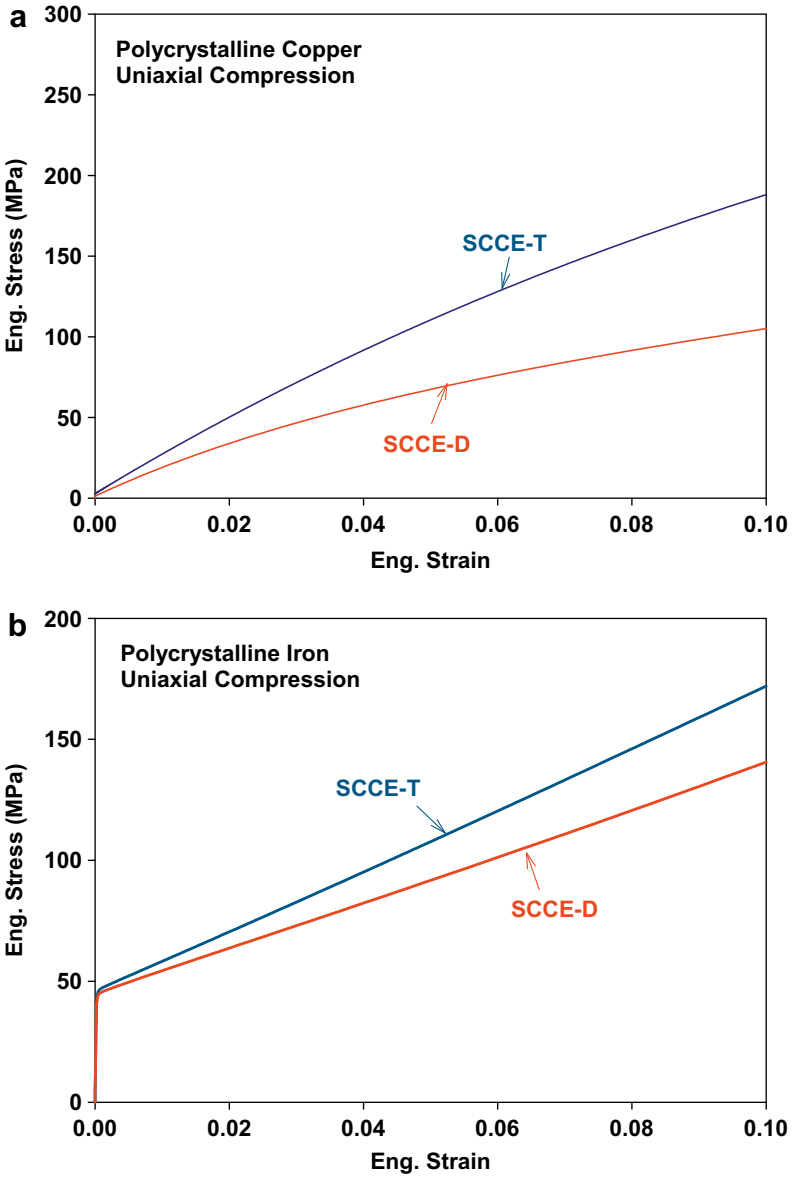

Fig. 9. Simulated macroscopic engineering stress–strain curves for uniaxial compression for (a) polycrystal copper, and (b) polycrystal iron.

throughout the tested strain range. Recall that both constitutive models were fit to single crystals oriented for multiple slip. As Figs. 3 and 4 illustrate, the SCCE-T model over-predicts the single crystal tensile flow stress for single slip and cases having limited numbers of slip systems. This over-prediction is apparently important for large polycrystal arrays; that is, regions of single or limited numbers of slip systems must still be present, thereby influencing the observed macro behavior, for macroscopic applied strains up to 0.1.

Figs. 10 and 11 shows predicted texture evolution for uniaxial tension and compression, respectively. Each pole figure is chosen to represent the major texture component in simple tension and compression for FCC and BCC, respectively. Simulated textures for both models show that the texture evolution in polycrystalline material has little sensitivity to the single crystal constitutive equations for both tension and compression.

3.4. Role of q_{lat}/q_{self} in SCCE-T

As noted above, a fixed value of $\mathbf{q_{lat}/q_{self} = 1.4}$ within the SCCE-T approach has been used with success for texture calculations in the literature and it is this implementation that has been assessed in the current work. In order to illuminate the role of $\mathbf{q_{lat}/q_{self}}$ in SCCE-T, a few additional fits and simulations were performed for copper single crystals. First, modified SCCE-T's were fit using alternate values of $\mathbf{q_{lat}/q_{self}}$ = 1.0, 1.2, 1.4 (standard value), 2.0, 3.0, and 50. The standard errors of fit for [0 0 1] tension were identical (0.67 MPa) for all tested values except those for $\mathbf{q_{lat}/q_{self}}$ =3.0 and 50 which were larger (0.95 and 2.23 MPa, respectively). For fits to [−1 2 3] tension, the standard error of fit for $\mathbf{q_{lat}/q_{self} = 1.4}$ was the minimum (2.1 MPa). Therefore, the best fits of SCCE-T with an arbitrarily adjustable value of $\mathbf{q_{lat}/q_{self}}$ gave the same "best" value as used above (and as endorsed by the literature). It should be noted that the modified SCCE-T used 5 adjustable parameters as compared with the 3 for SCCE-D, thus making the comparison increasingly biased in favor of SCCE-T.

As an extension of these tests, the various constitutive models (i.e. best-fit parameters for each choice of $\mathbf{q_{lat}/q_{self}}$) were then used to simulate tension tests carried out in the direction not used for fitting. The standard deviations for [−1 2 3] tensile tests simulated using the modified SCCE-T's were 20–68 MPa (160–540%), as compared with 10 MPa for SCCE-D (80%). The standard deviations for [0 0 1] tensile tests simulated using the modified SCCE-T's were 45–64 MPa (60–85%), as compared with 38 MPa for SCCE-D (50%). Thus, even using the more flexible SCCE-T with arbitrarily adjustable $\mathbf{q_{lat}/q_{self}}$ **(five** parameters) over a wide range of values did not match the accuracy of the fit or predictions obtained with the proposed SCCE-D (three parameters).

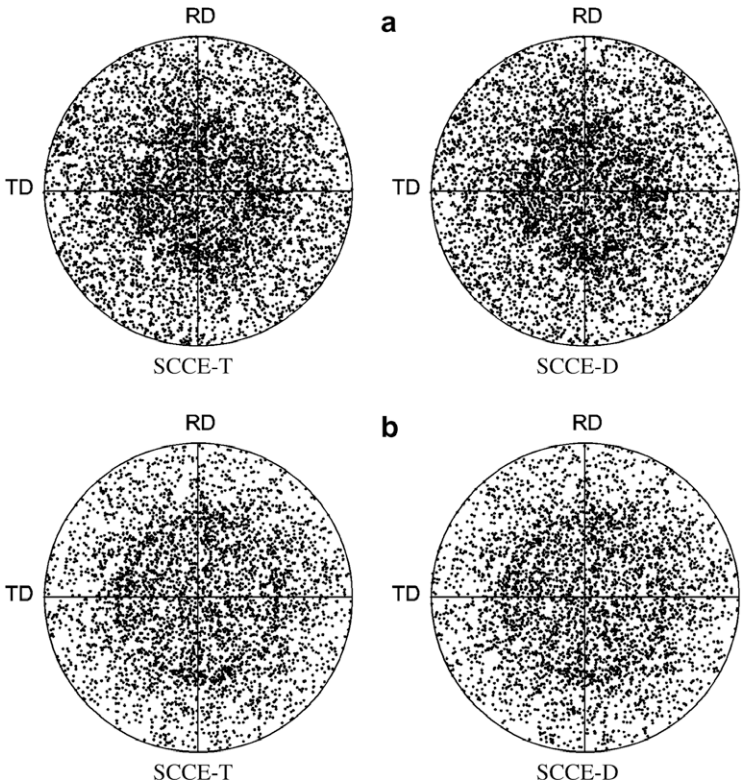

Fig. 10. Equal area projection pole figures after 50% tension; (a) {1 1 0} pole figure for copper, and (b) {1 1 1} pole figure for iron.

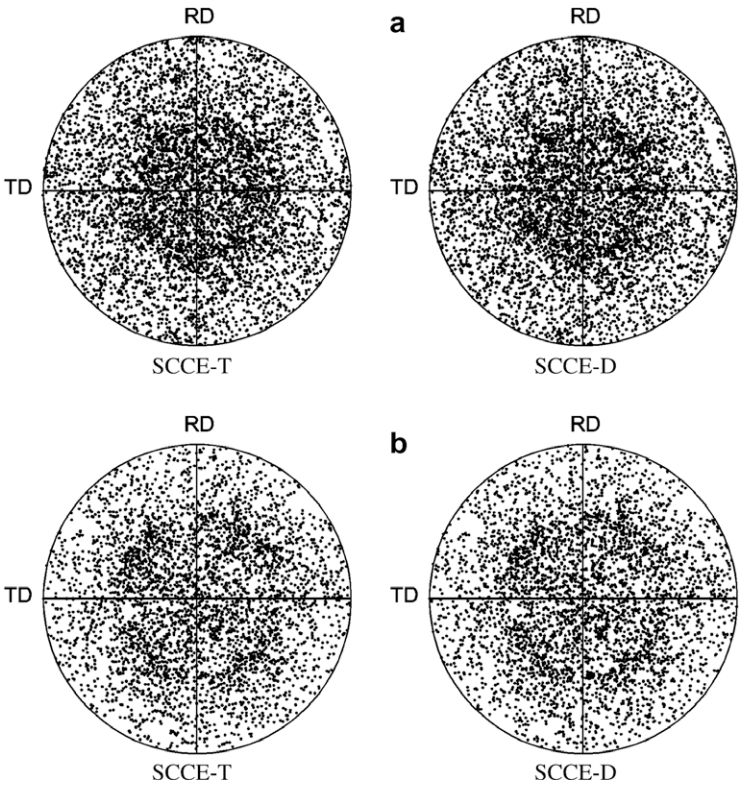

Fig. 11. Equal area projection pole figures after 50% compression; (a) {1 1 0} pole figure for copper, and (b) {1 1 1} pole figure for iron.

4. Conclusions

The following conclusions apply to comparisons of new Single Crystal Constitutive Equations based on Dislocation Density (SCCE-D) and standard Single Crystal Constitutive Equations for Texture Analysis (SCCE-T):

(1) SCCE-D reproduce flow curves for single slip and multi slip adequately in FCC and BCC single crystals. SCCE-D have better accuracy than SCCE-T while using smaller number of adjustable parameters. The average standard deviation predicted by SCCE-D is 14 MPa while that for the SCCE-T is 31 MPa.
(2) SCCE-T, which are usually back-fitted from polycrystal flow curves, do not adequately represent orientation - dependent single crystal behavior. The discrepancy may arise from neglecting the effect of grain boundaries, grain size and relative misorientations between grains.
(3) Polycrystal simulations using SCCE-T fit to multiple slip single crystal data predict higher flow stresses than SCCE-D, correlated with the high flow stresses predicted by the former for single crystals oriented for limited slip system activation. This correlation implies that there may exist significant regions of limited slip activation in polycrystals, contrary to the usual assumption.
(4) Texture evolution has little sensitivity to the type of constitutive equations. Simulated textures for SCCE-T and SCCE-D for FCC and BCC polycrystals are similar, while the simulated macroscopic stress–strain responses differ.

Acknowledgement

This work was sponsored by contract No. FA9550-05-0068 with Air Force Office of Scientific Research.

References

Abu Al-Rub, R.K., Voyiadjis, G.Z., 2005. A direct finite element implementation of the gradient-dependent theory. Int. J. Numer. Meth. Engng. 63, 603–629.
Alcalá, J., Casals, O., Očenášek, J., 2008. Micromechanics of pyramidal indentation in FCC metals: Single crystal plasticity finite element analysis. J. Mech. Phys. Solids. 56, 3277–3303.
Anand, L., Kothari, M., 1996. A computational procedure for rate-independent crystal plasticity. J. Mech. Phys. Solids 44, 525.
Arsenlis, A., Parks, D.M., 2002. Modeling the evolution of crystallographic dislocation density in crystal plasticity. J. Mech. Phys. Solids 50, 1979.
Asaro, R.J., 1979. Geometrical effects in the inhomogeneous deformation of ductile single crystals. Acta. Metall. 27, 445.
Asaro, R.J., 1983. Micromechanics of crystals and polycrystals. Adv. Appl. Mech. 23, 1–115.
Asaro, R.J., Needleman, A., 1985. Texture development and strain hardening in rate dependent polycrystals. Acta Metall. 33, 923–953.

Asaro, R.J., Rice, J.R., 1977. Strain localization in ductile single crystals. J. Mech. Phys. Solids 25, 309–338.
Bassani, J.L., Wu, T.Y., 1991. Latent hardening in single crystals. ii. Analytical characterization and predictions. Proc. R. Soc. Lond. A 435, 21.
Beaudoin, A.J., Dawson, P.R., Mathur, K.K., Kocks, U.F., Korzekwa, D.A., 1994. Application of polycrystal plasticity to sheet forming. Comput. Meth. Appl. Mech. Eng. 117, 49–70.
Becker, R., Panchanadeeswaran, S., 1995. Effects of grain interactions on deformation and local texture in polycrystals. Acta Metall. Mater. 43, 2701.
Bronkhorst, C.A., Kalidinidi, S.R., Anand, L., 1992. Polycrystalline plasticity and the evolution of crystallographic texture in FCC metals. Philos. Trans. Roy. Soc. Lond. A 341, 443.
Brown, S.B., Kim, K.H., Anand, L., 1989. An internal variable constitutive model for hot working of metals. Int. J. Plasticity 5, 95–130.
Canova, G.R., Kocks, U.F., Tome, C.N., Jonas, J.J., 1985. The yield surface of textured polycrystals. J. Mech. Phys. Solids 33, 371–397.
Dawson, P.R., 2000. Computational crystal plasticity. Int. J. Solids Struct. 37, 115–130.
Dawson, P.R., MacEwen, S.R., Wu, P.D., 2003. Advances in sheet metal forming analyses, dealing with mechanical anisotropy from crystallographic texture. Int. Mater. Rev. 48 (2), 86–122.
Franciosi, P., Zaoui, A., 1982. Multislip in F.C.C crystals: a theoretical approach compared with experimental data. Acta Metall. 30, 1627.
Hibbit, K.S.I., 2005. ABAQUS/Standard User's Manual.
Hill, R., 1966. Generallized constitutive relations for incremental deformation of metal crystals by multislip. J. Mech. Phys. Solids 14, 95.
Hill, R., Rice, J.R., 1972. Constitutive analysis of elastic plastic crystals at arbitrary strain. J. Mech. Phys. Solids 20, 401.
Hirth, J.P., Lothe, J., 1969. Theory of Dislocations. McGraw-Hill, New York.
Hutchinson, J.W., 1976. Bounds and Self-consistent Estimates for Creep of Polycrystalline Materials. Proc. R. Soc., London.
Kalidindi, S.R., Bronkshorst, C.A., Anand, L.J., 1992. Crystallographic texture evolution in bulk deformation processing of FCC metals. J. Mech. Phys. Solids 40, 537.
Keh, A.S., 1965. Work hardening and deformation sub-structure in iron single crystals deformed in tension at 298 K. Phil. Mag. 12, 9.
Kocks, U.F., 1970. The relation between polycrystal deformation and single crystal deformation. Metall. Trans. 1, 1121–1143.
Kocks, U.F., 1976. Laws for work-hardening and low-temperature creep. J. Engng Mater. Tech. (ASME H) 98, 76.
Kröner, 1961. Zur Plastichen Verformung des Vielkristalls. Acta Metall. 9, 155.
Kuchnicki, S.N., Cuitiño, A.M., Radovitzky, R.A., 2006. Efficient and robust constitutive integrators for single-crystal plasticity modeling. Int. J. Plasticity 22, 1988–2011.
Kumar, A., Dawson, P.R., 1998. Modeling crystallographic texture evolution with finite elements over neo-Eulerian orientation spaces. Comput. Meth. Appl. Mech. Eng. 153, 259.
Kumar, A.V., Yang, C., 1999. Study of work hardening models for single crystals using three dimensional finite element analysis. Int. J. Plasticity 15, 737.
Lee, E.H., 1969. Elastic–plastic deformation at finite strains. J. Appl. Mech. 36, 1.
Liu, Y., Varghese, S., Ma, J., Yoshino, M., Lu, H., Komanduri, R., 2008. Orientation effects in nanoindentation of single crystal copper. Int. J. Plasticity 24, 1990–2015.
Liu, Y., Wang, B., Yoshino, M., Roy, S., Lu, H., Komanduri, R., 2005. Combined numerical simulation and nanoindentation for determining mechanical properties of single crystal copper at mesoscale. J. Mech. Phys. Solids 53 (12), 2718–2741.
Ma, A., Roters, F., Raabe, D., 2004. A constitutive model for FCC single crystals based on dislocation densities and its application to uniaxial compression of aluminum single crystals. Acta Mater. 52, 3603–3612.
Ma, A., Roters, F., Raabe, D., 2006. A dislocation density based constitutive model for crystal plasticity FEM including geometrically necessary dislocations. Acta Mater. 54, 2169–2179.
Mandel, J., 1965. Generalization de la theorie de la plasticite de W.T. Koiter. Int. J. Solid Struct. 1, 273.
Marin, E.B., Dawson, P.R., 1998. On modeling the elasto-viscoplastic response of metals using polycrystal plasticity. Comput. Meth. Appl. Mech. Eng. 165 (1–4), 1–21.
Mathur, K.K., Dawson, P.R., 1989. On modeling the development of crystallographic texture in bulk forming precesses. Int. J. Plasticity 5, 67–94.
Molinari, A., Canova, G.R., Ahzi, S., 1987. A self consistent approach of the large deformation polycrystal viscoplasticity. Acta Metall. 35, 2983–2994.
Nakamachi, E., Xie, C.L., Harimoto, M., 2001. Drawbility assessment of BCC steel sheet by using elastic/crystalline viscoplastic finite element analyses. Int. J. Mech. Sci. 43, 631–652.
Nemat-Nasser, S., Ni, L.Q., Okinaka, T., 1998. A constitutive model for FCC crystals with application to polycrystalline OFHC copper. Mech. Mater. 30, 325.
Orowan, E., 1940. Problems of plastic gliding. Proc. Phys. Soc. 52, 8–22.
Orowan, E., 1948. Symposium on Internal Stresses in Metals and Alloys. The Institute of Metals, London. 451–453.
Ortiz, M., Popov, E., 1982. A statistical theory of polycrystalline plasticity. Comput. Meth. Appl. Mech. Eng. 90, 781.
Ortiz, M., Repetto, E.A., Stainer, L., 1999. A theory of subgrain dislocation structures. J. Mech. Phys. Solids 48, 2077–2114.
Parks, D.M., Ahzi, S., 1990. Polycrystalline plastic deformation and texture evolution for crystals lacking five independent slip systems. J. Mech. Phys. Solids 38, 701–724.
Patil, S.D., Narasimhan, R., Biswas, P., Mishra, R.K., 2008. Crack tip fields in a single edge notched aluminum single crystal specimen. J. Eng. Mater. Technol. 130 (2), 021013-1–021013-11.
Peirce, D., Asaro, R.J., Needleman, A., 1982. An analysis of nonuniform and localized deformation in ductile single crystals. Acta Metall. 30, 1087.
Raabe, D., Klose, P., Engl, B., Imlau, K.P., Friedel, F., Roters, F., 2002. Concepts for integrating plastic anisotropy into metal forming simulation. Adv. Eng. Mater. 4 (4), 169–180.
Raabe, D., Ma, D., Roters, F., 2007. Effects of initial orientation, sample geometry and friction on anisotropy and crystallographic orientation changes in single microcompression deformation: a crystal plasticity finite element study. Acta. Mater. 55, 4567–4583.
Rice, J.R., 1971. Inelastic constitutive relations for solids: an internal-variable theory and its application to metal plasticity. J. Mech. Phys. Solids 19, 433.
Roters, F., Raabe, D., Gottstein, G., 2000. Work hardening in heterogeneous alloys alloys – a microstructural approach based on three internal state variables. Acta Mater. 48, 4181–4189.
Sachs, G., 1928. Zur Ableitung Einer Fliessbedingung. Z. Ver. Dtsch. Ing. 72, 734–736.
Simmons, G., Wang, H., 1971. Single Crystal Elastic Constants and Calculated Aggregate Properties. The MIT Press, Cambridge, MA.
Takeuchi, T., 1975. Work hardening of copper single crystals with multiple glide orientation. Trans. Jpn. Inst. Metals 62, 307.
Taylor, G.I., 1938. Plastic Strain in Metals. J. Inst. Metals 62, 307.
Thakare, A.G., Narasimhan, R., Mishra, R.K., 2009. Numerical simulations of void growth near a notch tip in ductile single crystals. Mech. Mater. 41, 506–519.
Wang, H., Hwang, K.C., Huang, Y., Wu, P.D., Liu, B., Ravichandran, G., Han, C.-S., Gao, H., 2007. A conventional theory of strain gradient crystal plasticity based on the Taylor dislocation model. Int. J. Plasticity 23, 1540–1554.
Wang, Y., Raabe, D., Kluber, C., Roters, F., 2004. Orientation dependence of nanoindentation pile-up patterns and of nanoindentation microtextures in copper single crystals. Acta. Mater. 52, 2229–2238.
Weertman, J., Weertman, J.R., 1992. Elementary Dislocation Theory. Oxford Univ. Press.
Zaafarani, N., Raabe, D., Klüber, C., Roters, F., Zaefferer, S., 2006. Three dimensional investigation of the texture and microstructure below a nanoindent in a Cu single crystal using 3D EBSD and crystal plasticity finite element simulations. Acta. Mater. 54, 1707–1994.
Zaefferer, S., Kuo, J.-C., Zhao, Z., Winning, M., Raabe, D., 2003. On the influence of the grain boundary misorientation on the plastic deformation of aluminum bicrystals. Acta. Mater. 51, 4719–4735.